Geosci. Model Dev. Discuss., 8, 9925–9963, 2015
www.geosci-model-dev-discuss.net/8/9925/2015/
doi:10.5194/gmdd-8-9925-2015

Geoscientific Model Development Discussions
Open Access
EGU

Large ensemble modeling of last deglacial retreat of the West Antarctic Ice Sheet: comparison of simple and advanced statistical techniques

D. Pollard[1], W. Chang[2], M. Haran[3], P. Applegate[1,4], and R. DeConto[5]

[1]Earth and Environmental Systems Institute, Pennsylvania State University, University Park, USA
[2]Department of Statistics, University of Chicago, IL, USA
[3]Department of Statistics, Pennsylvania State University, University Park, USA
[4]Earth Sciences Program, Pennsylvania State University, DuBois, USA
[5]Department of Geosciences, University of Massachusetts, Amherst, USA

Received: 22 October 2015 – Accepted: 29 October 2015 – Published: 12 November 2015

Correspondence to: D. Pollard (pollard@essc.psu.edu)

Published by Copernicus Publications on behalf of the European Geosciences Union.

Abstract

A 3-D hybrid ice-sheet model is applied to the last deglacial retreat of the West Antarctic Ice Sheet over the last ∼ 20 000 years. A large ensemble of 625 model runs is used to calibrate the model to modern and geologic data, including reconstructed grounding lines, relative sea-level records, elevation-age data and uplift rates, with an aggregate score computed for each run that measures overall model-data misfit. Two types of statistical methods are used to analyze the large-ensemble results: simple averaging weighted by the aggregate score, and more advanced Bayesian techniques involving Gaussian process-based emulation and calibration, and Markov chain Monte Carlo. Results for best-fit parameter ranges and envelopes of equivalent sea-level rise with the simple averaging method agree quite well with the more advanced techniques, but only for a large ensemble with full factorial parameter sampling. Best-fit parameter ranges confirm earlier values expected from prior model tuning, including large basal sliding coefficients on modern ocean beds. Each run is extended 5000 years into the "future" with idealized ramped climate warming. In the majority of runs with reasonable scores, this produces grounding-line retreat deep into the West Antarctic interior, and the analysis provides sea-level-rise envelopes with well defined parametric uncertainty bounds.

1 Introduction

Modeling studies of future variability of the Antarctic Ice Sheet have focused to date on the Amundsen Sea Embayment (ASE) sector of West Antarctica, including the Pine Island and Thwaites Glacier basins. These basins are currently undergoing rapid thinning and acceleration, producing the largest Antarctic contribution to sea level rise (Shepherd et al., 2012; Rignot et al., 2014). The main cause is thought to be increasing oceanic melt below their floating ice shelves, which reduces back pressure on the grounded inland ice (buttressing; Pritchard et al., 2012; Dutrieux et al., 2014). There

GMDD
8, 9925–9963, 2015

is a danger of much more drastic grounding-line retreat and sea-level rise in the future, because bed elevations in the Pine Island and Thwaites Glacier basin interiors deepen to depths of a kilometer or more below sea level, potentially allowing Marine Ice Sheet Instability (MISI) due to the strong dependence of ice flux on grounding-line depth (Weertman, 1974; Mercer, 1978; Schoof, 2007; Vaughan, 2008; Rignot et al., 2014; Joughin et al., 2014).

Recent studies have mostly used high-resolution models and/or relatively detailed treatments of ice dynamics (higher order or full Stokes dynamical equations; Morlighem et al., 2010; Gladstone et al., 2012; Cornford et al., 2013; Parizek et al., 2013; Docquier et al., 2014; Favier et al., 2014; Joughin et al., 2014). Because of this dynamical and topographic detail, models with two horizontal dimensions have been confined spatially to limited regions of the ASE and temporally to durations on the order of centuries to one millennium. On the one hand, these types of models are desirable because highly resolved bed topography and accurate ice dynamics near the modern grounding line could well be important on timescales of the next few decades to century (references above, and Durand et al., 2011; Favier et al., 2012). On the other hand, the computational run-time demands of these models limit their applicability to small domains and short time scales, and they can only be calibrated against the modern observed state and decadal trends at most.

Here we take an alternate approach, using a relatively coarse-grid ice sheet model with hybrid dynamics. This allows run durations of many 1000's years, so that model parameters can be calibrated against geologic data of major retreat across the continental shelf since the Last Glacial Maximum (LGM) over the last ~ 20 000 years. The approach is a trade-off between (i) less model resolution and dynamical fidelity, which degrades future predictions on the scale of ~ 10's km and the next few decades (sill-to-sill retreat immediately upstream from modern grounding lines), and (ii) more confidence on larger scales of 100's km and 1000's years (deeper into the interior basins, further into the future) provided by calibration vs. LGM extents and deglacial retreat of the past 20 000 years. Also the approach allows more thorough exploration of uncertain

GMDD
8, 9925–9963, 2015

parameter ranges and their interactions, such as sliding coefficients on modern ocean beds, oceanic melting strengths, and different Earth treatments of bedrock deformation.

A substantial body of geologic data is available for the last deglacial retreat in the ASE and other Antarctic sectors. Notably this includes recent reconstructions of grounding-line locations over the last 25 kyrs (RAISED, 2014). Other types of data at specific sites include relative sea-level records, cosmogenic elevation-age data, and modern uplift rates (compiled in RAISED, 2014; Briggs and Tarasov, 2013; Briggs et al., 2013, 2014; Whitehouse et al., 2012a, b). Following several recent Antarctic modeling studies (Briggs et al. and Whitehouse et al. as above; Golledge et al., 2014; Maris et al., 2015), we utilize these datasets in conjunction with large ensembles (LE), i.e., sets of hundreds of simulations over the last deglacial period with systematic variations of selected model parameters. LE studies have also been performed for past variations of the Greenland Ice Sheet, for instance by Applegate et al. (2012) and Stone et al. (2013).

This paper follows on from Chang et al. (2015a, b), who apply relatively advanced Bayesian statistical techniques to LE's generated by our ice-sheet model. The statistical steps are described in detail in Chang et al. (2015a), and include:

- Statistical emulators, used to interpolate results in parameter space, constructed using a new emulation technique based on principal components.
- Probability models, replacing raw root-mean-square-error (RMSE) model-data misfits with formal likelihood functions, using a new approach for binary spatial data such as grounding-line maps.
- Markov Chain Monte Carlo (MCMC) methods, used to produce posterior distributions which are continuous probability density functions of parameter estimates and projected results based on formally combining the information from the above two steps in a Bayesian inferential framework.

Some of these techniques were applied to LE modeling for Greenland in Chang et al. (2014). McNeall et al. (2013) used a Gaussian process emulator, and scoring

GMDD
8, 9925–9963, 2015

similar to our simple method, in their study of observational constraints for a Greenland ice sheet model ensemble. Tarasov et al. (2012) used Artificial Neural Nets in North American ice-sheet modeling to fill in parameter space between LE simulations, and have mentioned their potential application to Antarctica (Briggs and Tarasov, 2013). Apart from these examples, to our knowledge the statistical techniques in Chang et al. (2015a, b) are considerably more advanced than the simpler averaging method used in most previous LE ice-sheet studies; these previous studies have involved (i) Computing a single objective score for each LE member that measures the misfit between the model simulation and geologic and modern data, and (ii) Calculating parameter ranges and envelopes of model results by straightforward averaging over all LE members, weighted by the scores.

The more advanced statistical techniques offer substantial advantages over the simple averaging method, such as providing robust and smooth probability density functions in parameter space. As shown in Applegate et al. (2012) and Chang et al. (2014), the simple averaging method fails to provide reasonable results for LE's with coarsely spaced Latin HyperCube sampling, whereas emulation and the other advanced steps successfully interpolate in parameter space, and provide smooth and meaningful probability densities.

However, the advanced techniques in Chang et al. (2015a, b) require statistical expertise not readily available to most ice-sheet modeling groups. It may be that the simple averaging method still gives reasonable results, especially for LE's with full factorial sampling, i.e., with every possible combination of selected parameter values (also referred to as grid or Cartesian product; Urban and Fricker, 2010). The purpose of this paper is to apply both the advanced statistical and simple averaging methods to the same Antarctic LE, compare the results, and thus assess whether the simple (and commonly used) method is a viable alternative to the more advanced techniques, at least for full factorial LEs. The results include probabilistic ranges of model parameter values, and envelopes of model results such as equivalent sea-level rise.

GMDD
8, 9925–9963, 2015

Section 2.1 and 2.2 describes the model, the setup for the last deglacial simulations, and the model parameters chosen for the full factorial LE. Section 2.3–5 describes the objective scoring vs. past and modern data used in the simple averaging method, and data used in the advanced statistical techniques. Results are shown for best-fit model parameter ranges and equivalent sea-level envelopes in Sects. 3 and 4, comparing simple and advanced techniques. Conclusions and steps for further work are described in Sect. 5.

2 Methods

2.1 Ice sheet model and simulations

The 3-D ice-sheet model has previously been applied to past Antarctic variations in Pollard and DeConto (2009), DeConto et al. (2012) and Pollard et al. (2015a). The model predicts ice thickness and temperature distributions, evolving due to slow deformation under its own weight, and to mass addition and removal (precipitation, basal melt and runoff, oceanic melt, and calving of floating ice). Floating ice shelves and grounding-line migration are included. It uses hybrid ice dynamics and an internal condition on ice velocity at the grounding line (Schoof, 2007). The simplified dynamics (compared to full Stokes or higher-order) captures grounding-line migration reasonably well (Pattyn et al., 2013), while still allowing O (10 000's) year runs to be feasible. As in many long-term ice sheet models, bedrock deformation is modeled as an elastic lithospheric plate above local isostatic relaxation. Details of the model formulation are described in Pollard and DeConto (2012a, b). The drastic ice-retreat mechanisms of hydrofracturing and ice-cliff failure proposed in Pollard et al. (2015a) are not included here, but will be combined with LE's in Pollard et al. (2015b).

The model is applied to a limited area nested domain spanning all of West Antarctica, with a 20 km grid resolution. Lateral boundary conditions on ice thicknesses and velocities are provided by a previous continental-scale run. The model is run over the

GMDD
8, 9925–9963, 2015

last 30 000 years, initialized appropriately at 30 ka (30 000 years before present, relative to 1950 AD) from a previous longer-term run. Atmospheric forcing is computed using a modern climatological Antarctic dataset (ALBMAP: Le Brocq, 2010), with uniform cooling perturbations proportional to a deep-sea core δ^{18}O record (as in Pollard and DeConto, 2009, 2012a). Oceanic forcing uses archived ocean temperatures from a global climate model simulation of the last 22 kyr (Liu et al., 2009). Sea level variations vs. time, which are controlled predominantly by Northern Hemispheric ice sheet variations, are prescribed from the ICE-5G dataset (Peltier, 2004). Modern bedrock elevations are obtained from the Bedmap2 dataset (Fretwell et al., 2013).

Each simulation is run from 30 ka to the present, and is extended 5000 years into the "future" with a very simple prescribed warming. Atmospheric and oceanic temperatures are uniformly increased by 6 and 2 °C, respectively, ramped linearly from the present to 150 years AP (after present) and held constant thereafter. Ocean-temperature increases are confined to a longitudinal sector (90 to 120^{o} W) enclosing the Amundsen Sea Embayment of West Antarctica, corresponding to the main region of observed sub-ice-shelf melt increases in recent decades. This simple prescription of future temperatures produces MISI and drastic ice retreat into the West Antarctic interior in many of the runs (as in Pollard and DeConto, 2009). More realistic future warming scenarios are planned for future work.

2.2 Large ensemble and model parameters

The large ensemble analyzed in this study uses full factorial sampling, i.e., a run for every possible combination of parameter values, with 4 parameters varied and with each parameter taking 5 values, requiring 625 (= 5^4) runs. As discussed above, results are analyzed in two ways: (1) using the relatively advanced statistical techniques (emulators, likelihood functions, MCMC) in Chang et al. (2015a, b), and (2) using the much simpler averaging method of calculating an aggregate score for each run that measures model-data misfit, and computing results as averages over all runs weighted by their score. Because the second method has no means of interpolating results between

GMDD
8, 9925–9963, 2015

sparsely separated points in multi-dimensional parameter space, it is effectively limited to full factorial sampling with only a few parameters and a small number of values each. The small number of values is nevertheless sufficient to span the full reasonable "prior" range for each parameter, and although the results are very coarse with the second method, they show the basic patterns adequately.

The 4 parameters were chosen based on prior experience with the model; each has a strong effect on the results, yet their values are particularly uncertain. They are listed along with their values in the box below (Listing 1). The first 3 involve oceanic processes or properties of modern ocean-bed areas. Parameters whose effects are limited to modern grounded-ice areas are reasonably well constrained by earlier work, such as basal sliding coefficients under modern grounded ice which are obtained by inverse methods (e.g., Pollard and DeConto, 2012b, for this model). More discussion of the physics and uncertainties associated with these parameters is given in Appendix A.

2.3 Individual data types and scoring

Following Whitehouse (2012a, b), Briggs and Tarasov (2013) and Briggs et al. (2013, 2014), we test the model against 3 types of data for the modern observed state, and 5 types of geologic data relevant to ice-sheet variations of the last ~ 20 000 years, using straightforward root-mean-square (RMSE) misfits in most cases. Each misfit (M_i, i = 1 to 8) is normalized into an individual score (S_i), which are then combined into one aggregate score (S) for each member of the LE. Only data within the domain of the model (West Antarctica) is used in the calculation of the misfits.

We first describe the full calculation used in the simple averaging method. The 8 individual data types and model-data misfits are outlined in the box below (Listing 2), with more details given in Appendix B, followed by the method of combining them into one aggregate score S. The more advanced statistical techniques (Chang et al., 2015a, b) use elements of these calculations, but differ fundamentally in some aspects, as discussed further below.

GMDD
8, 9925–9963, 2015

2.4 Combination into one aggregate score for simple averaging method

Each of the RMSE or χ-squared misfits above are first transformed into a normalized individual score for each data type $i = 1$ to 8, as follows. A "cutoff" value C_i is set by taking the geometric mean (i.e., logarithmic mean, square root of the product) of (i) the minimum (best) RMSE value over all the LE runs, and (ii) the algebraic average of the 10 largest (worst) values. The 10 worst values are used to avoid a single outlier that could be unbounded; the single best value is used because it is bounded by zero, and is not an outlier but represents close-to-the-best possible simulation with the current model. The geometric mean and not the algebraic mean of these two numbers is more appropriate if the values range over many orders of magnitude.

The individual score $S_i = \max[0, \min[1, 1 - M_i/C_i]]$, for each ensemble run and for each data type $i = 1$ to 8. Each M_i and C_i is a recognizable physical quantity or ratio, and if $M_i > C_i$, the simulation is definitely very poor, not even resembling the appropriate data. S_i values close to 1 ($M_i \ll C_i$) represent very good simulations of this data type, close to the best possible within the LE. S_i values of 0 ($M_i \geq C_i$) represent very bad simulations, diverging from this data type so much that the run should be rejected no matter what the other scores are.

Then the geometric (logarithmic) average of the 8 individual S_i's is taken to yield the aggregate score S for each run:

$$S = (S_1 S_2 S_3 S_4 S_5 S_6 S_7 S_8)^{1/8}$$

This formula (as opposed to the algebraic mean of the S_i for instance) means that if any individual score is 0, then S is zero. It corresponds to the notion that if any single data type is completely mismatched, the run should be rejected as unrealistic, regardless of the fit to the other data types. It differs from the weighting in Briggs and Tarasov (2013) (their "inter-data-type"), which is algebraic and depends heavily (80 %) on the fit to modern ice distribution. Here we more heavily emphasize the fit to past data, even if more uncertain and sparser than modern, which seems pertinent to future simulations

GMDD
8, 9925–9963, 2015

with very large departures from modern conditions. Our overall approach has links to the calibration technique in Gladstone et al. (2012) and the more formal treatment in McNeall et al. (2013).

2.5 Advanced statistical techniques

The more advanced statistical techniques (Chang et al., 2015a, b) do not use the aggregate score S at all, but perform statistical emulation of modern and past grounding-line locations. Chang et al. (2015b) use exactly the same LE as here, applying statistical emulators, probability models and likelihood functions to (i) modern grounding-line geographical maps, and (ii) past locations of grounding lines vs. time along the centerline trough of Pine Island Glacier (replacing the data types TOTE, TROUGH and GL2D above).

For this paper, the advanced techniques are extended to additionally use the individual score values for the data types TOTI, TOTDH, RSL, ELEV/DSURF and UPL, (S_2, S_3, S_6, S_7, S_8). The raw data for these quantities are less amenable to emulation, especially those with site-specific records (RSL, ELEV/DSURF, UPL). The use of the individual scores is described in Appendix C.

3 Results: aggregate scores with simple averaging method

Figure 2 shows the aggregate scores S for all 625 members of the LE, over the 4-dimensional space of the parameters CSHELF, TAUAST, OCFAC and CALV. Each individual subpanel shows TAUAST vs. CSHELF, and the subpanels are arranged left-to-right for varying CALV, and bottom-to-top for varying OCFAC.

3.1 "Outer" variations, CALV and OCFAC

All scores with the largest CALV value of 1.7 (right-hand column of subpanels) are 0. In these runs, excessive calving results in very little floating ice shelves and far

GMDD
8, 9925–9963, 2015

too much grounding line-retreat. Conversely, with the smallest CALV value of 0.3 (left-hand column of subpanels), most runs have too much floating ice and too advanced grounding lines during the runs, so most of this column also has zero scores. However, small CALV can be partially compensated by large OCFAC (strong ocean melting), so there are some non-zero scores in the upper-left subpanels.

3.2 "Inner" variations, CSHELF and TAUAST

For mid-range CALV and OCFAC (subpanels near the center of the figure), the best scores require high CSHELF (inner x axis) values, i.e., slippery ocean-bed coefficients of 10^{-6} to 10^{-5} m a^{-1} Pa^{-2}. This is the most prominent signal in Fig. 2, and is consistent with the widespread extent of deformable sediments on continental shelves noted above. Ideally the LE should have included CSHELF values greater than 10^{-5}, but the model frequently proved to be numerically unstable in that range. In a subsequent paper this instability is avoided and a larger CSHELF range is explored (Pollard et al., 2015b). However, we note that values of 10^{-5} to 10^{-6} have been found to well represent active Siple Coast ice-stream beds in model inversions (Pollard and DeConto, 2012b).

Somewhat lower but still reasonable scores exist for lower CSHELF values of 10^{-7}, but only for higher OCFAC (3 to 10) and smaller TAUAST (1 to 2 kyr). This is of interest because smaller CSHELF values support thicker ice thicknesses at LGM where grounded ice has expanded over continental shelves, producing greater equivalent sea-level lowering and alleviating the LGM "missing-ice" problem (Clark and Tarasov, 2014). In order for the extra ice to be melted by present day, ocean melting needs to be more aggressive (higher OCFAC), and to recover in time from the greater bedrock depression at LGM, TAUAST has to be smaller (more rapid bedrock rebound). This region of parameter space is explored further in Pollard et al. (2015b).

Scores are quite insensitive to the asthenospheric rebound time scale TAUAST (inner y axis), although there is a tendency to cluster around 2 to 3 kyr and to disfavor higher values (5 to 7 kyr) especially for high OCFAC.

GMDD
8, 9925–9963, 2015

4 Results: comparisons of simple averaging vs. advanced statistical techniques

4.1 Single parameter ranges

The main results seen in Fig. 2 are borne out in Fig. 3. The left-hand panels show results using the simple averaging method, i.e., the average score for all runs in the LE with a particular parameter value. Triangles in these panels show the mean parameter value $V_m = \Sigma(S^{(n)}V^{(n)})/\Sigma S^{(n)}$, where $S^{(n)}$ is the aggregate score and $V^{(n)}$ is the value of this parameter for run n (1 to 625), and whiskers show the standard deviation. The prominent signal of high CSHELF values (slippery ocean beds) is evident, along with the absence (near absence) of positive scores for the extreme CALV values of 1.7 (0.3), and the more subtle trends for OCFAC and TAUAST.

The right-hand panels of Fig. 3 show the same single-parameter "marginal" probability density functions for this LE, using the advanced statistical techniques described in Chang et al. (2015a, b) and summarized above. For OCFAC, CSHELF and TAUAST, there is substantial agreement with the simple-averaging results in both the peak "best-fit" values and the width of the ranges. For CALV, the peak values agree quite well, but the simple-averaging distribution has a significant tail for lower CALV values that disagrees with zero probabilities in the advanced results. We will investigate this disagreement in further work.

4.2 Paired parameter ranges

Probability densities for pairs of parameter values are useful in evaluating the quality of LE analysis, and can display offsetting physical processes that together maintain realistic results, e.g., greater OCFAC and lesser CALV (Chang et al., 2014, 2015a, b). In Fig. 4, the left-hand panels show mean scores for pairs of the 4 parameters, using the simple averaging method and averaged over all LE runs with a particular pair of values. The right-hand panels show corresponding densities for the same parameter pairs us-

GMDD
8, 9925–9963, 2015

ing the advanced statistical techniques. Overall the same encouraging agreement is seen as for the single-parameter densities in Fig. 3, with the locations of the main maxima being roughly the same for each parameter pair. There are some differences in the extents of the maxima, notable for CALV where the zone of high scores with the simple averaging method extends to lower CALV values than with the advanced techniques, as seen for the individual parameters in Fig. 3. In general, though, there is good agreement between the two methods regarding parameter ranges in Figs. 3 and 4, suggesting that the simple averaging method is viable, at least for LE's with full factorial sampling of parameter space.

4.3 Past and future equivalent-sea-level change

Figure 5 illustrates the use of the LE to produce past and future envelopes of model predictions. Figure 5a, b show equivalent sea-level (ESL) scatter plots for all 625 runs. Early in the runs around LGM (20 to 15 ka), the curves cluster into noticeable groups with the same CSHELF values, due to the relatively weak effects of the other parameters (OCFAC, CALV and TAUAST) for cold climates and ice sheets in near equilibrium. Figure 5c and d shows the mean and one-sided standard deviations for the simple method. Most of the retreat and sea-level rise occurs between ~ 14 to 10 ka, and is somewhat more sudden and earlier than in other versions of the model due to a new feedback in the calving parameterization. This may be too strong and is re-evaluated in a subsequent paper (Pollard et al., 2015b).

Figure 5e, f shows the equivalent mean and standard deviations derived from the advanced statistical techniques. There is substantial agreement with the simple-method curves in Fig. 5c and d, for most of the duration of the runs. The largest difference is around the Last Glacial Maximum ~ 20 to 15 ka, when mean sea levels are up to ~ 2.5 m lower (larger LGM ice volumes) in the simpler method compared to the advanced. This may be due to the simpler method's scoring with past 2-D grounding-line reconstructions (GL2D data type), which are not used in the advanced technique; this difference will be examined further in ongoing work.

GMDD
8, 9925–9963, 2015

The majority of runs with reasonably good aggregate scores produce substantial "future" WAIS collapse, with Marine Ice Sheet Instability causing grounding-line retreat of the Pine Island and Thwaites glaciers into the West Antarctic interior. As seen in Fig. 5, this produces up to 2.6 m of equivalent sea-level (ESL) rise on several-century to thousand-year time scales (1.7 m after 1000 years, 2.6 after 5000 years), consistent with earlier model behavior in Pollard and DeConto (2009). Note that the prescribed "future" warming here is very simple, with linear ramps of all atmospheric and oceanic temperatures as described above. More detailed future climate-warming scenarios are explored using LE methods in Pollard et al. (2015b).

Figure 6 shows probability densities of equivalent sea level rise at particular times in the runs, including +500, +1000 and +5000 years after modern. Figure 6a–d show results with the simple averaging method, computed using score-weighted densities and 0.2 m wide ESL bins (see caption). The uneven noise in this figure is due to the small number of parameter values in our LE. The separate peaks for LGM (−15 000 yr) in Fig. 6a and b are due to the widely separated CSHELF values, and the relatively weak effects of the other parameters (OCFAC, CALV and TAUAST) for cold climates and ice sheets in near equilibrium. Figure 6e shows the equivalent but much smoother probability densities using the advanced statistical techniques, for the "future" times. There is fair agreement with the simple averaging results, including the skewed tendency at +5000 years.

5 Conclusions

1. The simple averaging method, with quantities weighted by RMSE-based aggregate scores, produces results that are reasonably compatible with sophisticated statistical techniques involving emulation, probability model/likelihood functions, and MCMC (Chang et al., 2015a, b; Sect. 2.5; Appendix C). However, we have shown this only for an LE with full factorial sampling in parameter space. Unlike the advanced techniques, the simple averaging method cannot interpolate in pa-

GMDD
8, 9925–9963, 2015

rameter space, and so is limited practically to relatively few parameters (4 here) and a small number of values for each (5 here). As shown in Chang et al. (2014), the simple averaging method fails to yield meaningful results for LEs with sparse LatinHyperCube sampling. In contrast, the advanced techniques permit Latin HyperCube sampling with at least ~ 10 parameters (Chang et al., 2015a), and produce robust and smooth probability densities for parameter values and modeled quantities as shown here.

2. The best-fit parameter ranges deduced from the LE analysis generally fit prior expectations. In particular, the results strongly confirm that large basal sliding coefficients (i.e., slippery beds) are appropriate for modern continental-shelf oceanic areas. In further work we will assess heterogeneous bed properties such as the inner region of hard outcropping basement observed in the ASE (Gohl et al., 2013).The best-fit range for the asthenospheric relaxation time scale TAUAST values is quite broad, including prior nominal values ~ 3 kyr, but extending to shorter times ~ 1 kyr. This may be connected with low upper-mantle viscosities and thin crustal thicknesses suggested in recent work (Whitehouse et al., 2012b; Chaput et al., 2014), which will be examined in further work with full Earth models (Gomez et al., 2013, 2015; Konrad et al., 2015).

3. Consistent with trends in recent Antarctic modeling studies (Ritz et al., 2001; Huybrechts, 2002; Philippon et al., 2006; Briggs et al., 2013, 2014; Whitehouse et al., 2012a, b; Golledge et al., 2012, 2013, 2014), the greater total Antarctic ice amount at the Last Glacial Maximum is less than in earlier papers, equivalent to ~ 5 to 10 m of global equivalent sea level below modern. (This contribution is only from our limited West Antarctic domain, but as shown in Macintosh et al., 2011, the contribution from East Antarctica at LGM is much smaller, ~ 1 m e.s.l.). This suggests that Antarctic expansion is insufficient to explain the "missing ice" problem, i.e., the total volume of reconstructed ice sheets worldwide is less than the equivalent fall in sea-level records at that time by 15 to 20 m (Clark and Tarasov, 2014).

GMDD
8, 9925–9963, 2015

A subsequent paper (Pollard et al., 2015b) uses a similar LE to evaluate the potential for greater LGM ice volumes.

4. There are only minor episodes of accelerated WAIS retreat and equivalent sea-level rise in the simulations (Fig. 5), and none with magnitudes comparable to Melt Water Pulse 1A for instance, with ~ 15 m e.s.l. rise in ~ 350 years around ~ 14.5 ka (Deschamps et al., 2012), in apparent conflict with significant Antarctic contribution implied by sea-level fingerprinting studies (Bassett et al., 2005; Deschamps et al., 2012) and IRD-core analysis (Weber et al., 2014). Model retreat rates are examined in more detail in Pollard et al. (2015b), where the potential for greater pulses is assessed by imposing episodes of ocean warming around 15 to 14 ka, similarly to Golledge et al. (2014).

5. One robust conclusion is that most parameter combinations with reasonable scores produce retreat deep into the West Antarctic interior in response to simple idealized "future" warming, causing up to ~ 2 to 3 m equivalent sea-level rise on several century to few millennia timescales. It is driven by Marine Ice Sheet Instability in WAIS basins, consistent with past retreats simulated in Pollard and DeConto (2009). DeConto and Pollard (2015) use more detailed future climate warming (Representative Concentration Pathways, Meinshausen et al., 2011), and also include drastic retreat mechanisms of hydrofracture and ice-cliff failure and another type of LE analysis. These aspects are combined with the LE methods described here in Pollard et al. (2015b).

Appendix A: Model parameters varied in the large ensemble

The four model parameters (OCFAC, CALV, CSHELF and TAUAST) and their ranges in the large ensemble are summarized in Sect. 2.2 above. Their physical effects in the model and associated uncertainties are discussed in more detail here.

GMDD
8, 9925–9963, 2015

OCFAC is the main coefficient in the parameterization of sub-ice-shelf oceanic melt, which is proportional to the square of the difference between nearby water temperature at 400 m, and the pressure-melting point of ice. Oceanic melting (or freezing) erodes (or grows on) the base of floating ice shelves, as warm waters at intermediate depths flow into the cavities below the shelves. The resulting ice-shelf thinning reduces pinning points and lateral friction, and thus back stress on grounded interior ice. As mentioned above, recent increases in ocean melt rates are considered to be the main cause of ongoing downdraw and acceleration of interior ice in the ASE sector of WAIS (Pritchard et al., 2012; Dutrieux et al., 2014). High-resolution dynamical ocean models (Hellmer et al., 2012) are not yet practical on these time scales, and simple parameterizations of sub-ice-shelf melting such as the one used here are quite uncertain (e.g., Holland et al., 2008). For small (large) OCFAC values, oceanic melting is reduced (increased), ice shelves thicken (thin), discharge of interior ice across the grounding line decreases (increases), and grounding lines tend to advance (retreat).

CALV is the main factor in the parameterization of iceberg calving at the oceanic edges of floating shelves. Calving has important effects on ice-shelf extent with strong feedback effects via buttressing of interior ice. However, the processes controlling calving are not well understood, probably depending on a combination of pre-existing fracture regime, large-scale stresses, and hydrofracturing by surface meltwater. There is little consensus on calving parameterizations. We use a common approach based on parameterized crevasse depths and their ratio to ice thickness (Benn et al., 2007; Nick et al., 2010). For small (large) CALV, calving is decreased (increased), producing more (less) extensive floating shelves, and greater (lesser) buttressing of interior ice.

CSHELF is the basal sliding coefficient for ice grounded on areas that are ocean bed today (and is not frozen to the bed). Coefficients under modern grounded ice are deduced by inverse methods (Pollard and DeConto, 2012b; Morlighem et al., 2013), but they are relatively unconstrained for modern oceanic beds, across which grounded ice advanced at the Last Glacial Maximum ~ 20 to 15 ka. Most oceanic beds around Antarctica are covered in deformable sediment today, due to Holocene marine sedi-

GMDD
8, 9925–9963, 2015

mentation, and to earlier transport and deposition of till by previous ice advances. For these regions, coefficients are expected to be relatively high (i.e., slippery bed), but there is still a plausible range that has significant effects on model results, because it strongly controls the steepness of the ice-sheet surface profile and ice thicknesses, and thus the sensitivity to climate change. In this paper, we vary the sliding coefficient CSHELF uniformly for all modern-oceanic areas. (In further work, we will allow for heterogeneity such as the hard crystalline bedrock zone observed in the inner Amundsen Sea Embayment; Gohl et al., 2013).

TAUAST is the e-folding time of asthenosephic relaxation in the bedrock model component. Ice sheet evolution on long timescales is affected quite strongly by the bedrock response to varying ice loads, especially for marine ice sheets in contact with the ocean where bathymetry determines grounding-line depths. During deglacial retreat, the bedrock rebounds upwards due to reduced ice load, which slows down ice retreat due to shallower grounding-line depths and less discharge of interior ice. However, the $O\,(10^3)$-year lag in this process is important in reducing this negative feedback, and accelerates the positive feedback of Marine Ice Sheet Instability if the bed deepens into the ice-sheet interior. As in many large-scale ice-sheet models, our bedrock response is represented by a simple Earth model consisting of an elastic plate over a local e-folding relaxation towards isostatic equilibrium (Elastic Lithosphere Relaxing Asthenosphere). Based on more sophisticated global Earth models, the asthenospheric e-folding time scale is commonly set to 3 kyr (e.g., Gomez et al., 2013), but note that recent geophysical studies suggest considerably shorter time scales for some West Antarctic regions (Whitehouse et al., 2012b; Chaput et al., 2014). In further work we plan to perform large ensembles with the ice sheet model coupled to a full Earth model, extending Gomez et al. (2013, 2015).

GMDD
8, 9925–9963, 2015

Appendix B: Data types and individual misfits

The 8 types of modern and past data used in evaluating the model simulations are summarized in Sect. 2.3 above. More details on the data and the algorithms used to compute the individual mismatches M_1 to M_8 with model quantities are given below. The term "domain" refers to the nested model grid that spans all of West Antarctica, and we only compare with observational sites and data within this domain. Modern observed data is from the Bedmap2 dataset (Fretwell et al., 2013).

1. TOTE: Modern grounding-line locations. The misfit M_1 is the total area of mismatch where model is grounded and observed is floating ice or ocean, or vice versa, relative to total area of the domain.

2. TOTI: Modern floating ice-shelf locations. The misfit M_2 is the total area of mismatch where model has floating ice and observed does not, or vice versa, relative to the total area of the domain.

3. TOTDH: Modern grounded ice thicknesses. The misfit M_3 is the RMS difference between model and observed ice thicknesses, over areas with observed modern grounded ice.

4. TROUGH: Past grounding-line distance vs. time along centerline troughs of Pine Island Glacier, and optionally the Ross and Weddell basins. Observed distances at ages 20, 15, 10 and 5 ka are obtained from grounding-line reconstructions of the RAISED Consortium (2014), using their Scenario A (most retreated ice) for the Weddell, and then linearly interpolated in time between these dates. The centerline trough for Pine Island Glacier is extended across the continental shelf following the paleo-ice-stream trough shown in Jakkobsen et al. (2011). The resulting Pine-Island transect vs. time is similar to that in Smith et al. (2014). The misfit M_4 is the RMS difference in model vs. observed grounding-line distance over the period 20 to 0 ka. In this study just the Pine Island Glacier trough is used, but if the

GMDD
8, 9925–9963, 2015

Ross and Weddell are used also, the RMS difference is calculated over all data points.

5. GL2D: Past grounding-line locations. This uses reconstructed grounding-line maps for 20, 15, 10, 5 ka (RAISED, 2014, with vertices provided by S. Jamieson, personal communication, 2014) and for modern (0 ka, Bedmap2, Fretwell et al., 2013). The past maps (RAISED, 2014) are only available around West Antarctica, so the calculations below do not include the East Antarctic margin for ensembles spanning the entire ice sheet. Furthermore, for this study only the Amundsen Sea region was used. We allow for uncertainty in the past reconstructions by setting a probability of floating ice or open ocean at each point P_{obs} as follows:

   i. Computing the distance D_1 from the reconstructed grounding line.

   ii. Dividing this distance by the sum D_2 of the (Kriged) reported uncertainty of nearby vertices (interpreting their "measured" = 10 km, "inferred" = 50 km, "speculative" = 100 km) and a distance that ramps up to 100 km depending on distance to the nearest vertex dv (i.e., $100\max[0, \min[1, (dv - 100)/200]]$), to obtain a scaled distance $D_s = D_1/D_2$.

   iii. Setting the probability P_{obs} to a value decaying upwards or downwards from 0.5, i.e., to $0.5\,e^{-Ds}$ if on the grounded side of the grounding line, or to $1 - 0.5\,e^{-Ds}$ if on the non-grounded side.

Then the mismatch at each model grid point is set to 2 $(0.5 - P_{obs})$ if $P_{obs} < 0.5$ and the model is not grounded, or 2 $(P_{obs} - 0.5)$ if $P_{obs} > 0.5$ and the model is grounded. The mismatch is zero if the model is not grounded anywhere on the non-grounded side of the observed grounding line, or if it is grounded anywhere on the grounded side. Thus, if the model and observed grounding lines coincide exactly everywhere, then the mismatch is zero at all points, regardless of the observational uncertainty reflected in P_{obs} (which seems a desirable feature). The

GMDD
8, 9925–9963, 2015

total misfit (M_5) is the areally weighted sum of the mismatches for all points in the domain, relative to total domain area.

6. RSL: Past Relative Sea Level (RSL) records. This uses the compilation by Briggs and Tarasov (2013) of published RSL data vs. time at sites around the modern coastline. Following those authors, a χ-squared measure vs. model output is computed, i.e., the sum of squared model minus observed δRSL for each site and time datum, divided by the observational RSL uncertainty, i.e., $(\delta\mathrm{RSL})^2/\sigma_{\mathrm{zo}}^2$. The model RSL = [SL($t$) – $h_{\mathrm{b}}(t)$] – [SL(0) – $h_{\mathrm{b}}(0)$], where SL(t) is global sea level (with t = 0 at modern) and h_{b} is bed elevation, at the closest model grid point to the observed site. The minimum difference δRSL is used, over all model times within the range of the observational time uncertainty ($t_{\mathrm{obs}} \pm \sigma_{\mathrm{to}}$). As in Briggs and Tarasov (2013), the elevation uncertainty σ_{zo} is much larger for one-sided constraints than absolute constraints (if the model is on the correct side). The sum of $(\delta\mathrm{RSL})^2/\sigma_{\mathrm{zo}}^2$ is taken over all observed sites and times to obtain the overall misfit M_6. To reduce the influence of many closely spaced sites, following Briggs and Tarasov (2013) an "intra-data-type weighting" is applied that is inversely proportional to the number of data points within a distance L of each other, where L is equivalent to 5° latitude (~ 550 km).

7. ELEV/DSURF: This uses a combination of two compilations of cosmogenic data: elevation vs. age in Briggs and Tarasov (2013) for ELEV, and thickness change from modern vs. age in RAISED (2014) for DSURF. For each observed datum, the model output at the closest grid point is used to find:

   – For ELEV: the minimum squared mismatch of ice elevation and time, within the constraints of descending elevation trend, each relative to the observational uncertainties of elevation and time.
   – For DSURF: the minimum mismatch in ice thickness change, within the range of observational time uncertainty, reduced by the observational thickness uncertainty.

GMDD
8, 9925–9963, 2015

Mismatches are averaged over all observed sites and times, weighted by intra-data-type weighting as described for RSL above. Mismatches (M_{7a}, M_{7b}) are calculated separately for ELEV and DSURF, and converted into separate normalized scores (S_{7a}, S_{7b}) as described above. The two separate scores are then combined into one by taking the square root of their product, i.e., $S_7 = (S_{7a}S_{7b})^{1/2}$.

8. UPL: This uses modern uplift rates on rock outcrops, using the compilation in Whitehouse et al. (2012b). For each observed site, the model's modern $\partial h_b/\partial t$ at the closest model grid point is used. The overall misfit M_8 is the RMS difference from observed, equally weighted (not using intra-data-type weighting or accounting for observational uncertainty).

Appendix C: Using individual scores in the advanced statistical techniques

This appendix describes the use of individual data-type scores (TOTI, TOTDH, RSL, ELEV/DSURF and UPL) in the advanced statistical techniques, as mentioned in Sect. 2.5.

Our two-stage approach consists of an emulation and a calibration stage. In the emulation stage we build separate statistical emulators for the modern and past grounding-line locations and the individual scores. For details of emulating the modern and past grounding-line locations we refer to Chang et al. (2015a,b). To use individual scores for particular data types, we build a Gaussian process emulator with a separable covariance structure between the input parameter settings and different scores. The covariance matrix for different input parameter settings is defined using an exponential covariance function, with parameters estimated by maximizing the likelihood function. The covariance matrix for the different score values is estimated as the sample covariance matrix computed from the LE, by treating different input parameter settings as replicates.

GMDD
8, 9925–9963, 2015

In the calibration stage we define the posterior densities of input parameters, based on modern and past grounding-line locations and the individual scores, to infer the input parameters based on those densities via Markov Chain Monte Carlo (MCMC) using the standard Metropolis–Hastings algorithm. Again, we refer to Chang et al. (2015a,b) for details of defining the posterior densities for modern and past grounding-line locations. To define the likelihood function based on the individual score values we use exponential marginal densities and a Gaussian copula. The rate parameter for each exponential density receives gamma prior with a shape parameter of 30 and a scale parameter specified in a way that the 90th percentile of the prior density coincides with the cutoff C_i (Sect. 2.4). The correlation matrix for the Gaussian copula is estimated as the sample rank correlations matrix for the individual score values in the LE, again by treating the different input parameter settings as replicates.

Code availability

The code for the ice-sheet model (PSUICE-3D) is available on request from D. Pollard (pollard@essc.psu.edu). The postprocessing codes for the large-ensemble statistical analyses are highly tailored to specific sets of model output and are not made available; however, modules that compute scores for the individual data types (Sect. 2.3, Appendix B) are available on request to pollard@essc.psu.edu.

Acknowledgements. We thank Zhengyu Liu and his group at U. Wisconsin for providing output of their coupled GCM simulation (TRACE; Liu et al., 2009; He et al., 2013) used for ocean forcing over the last 20 000 years. This work was supported in part by the following grants from the National Science Foundation: NSF-DMS-1418090 and the Network for Sustainable Climate Risk Management (SCRiM) under NSF cooperative agreement GEO1240507 (DP, MH); OCE-1202632, OPP-1341394 (DP); NSF Statistical Methods in the Atmospheric Sciences Network 1106862, 1106974, and 1107046 (WC).

GMDD
8, 9925–9963, 2015

References

Applegate, P. J., Kirchner, N., Stone, E. J., Keller, K., and Greve, R.: An assessment of key model parametric uncertainties in projections of Greenland Ice Sheet behavior, The Cryosphere, 6, 589–606, doi:10.5194/tc-6-589-2012, 2012.

Bassett, S. E., Milne, G. A., Mitrovica, J. X., and Clark, P. U.: Ice sheet and Solid Earth influences on far-field sea-level histories, Science, 309, 925–928, 2005.

Benn, D. I., Warren, C. R., and Mottram, R. H.: Calving processes and the dynamics of calving glaciers, Earth-Sci. Rev., 82, 143–179, 2007.

Briggs, R. D. and Tarasov, L.: How to evaluate model-derived deglaciation chronologies: a case study using Antarctica, Quaternary Sci. Rev., 63, 109–127, 2013.

Briggs, R., Pollard, D., and Tarasov, L.: A glacial systems model configured for large ensemble analysis of Antarctic deglaciation, The Cryosphere, 7, 1949–1970, doi:10.5194/tc-7-1949-2013, 2013.

Briggs, R. D., Pollard, D., and Tarasov, L.: A data-constrained large-ensemble analysis of Antarctic evolution since the Eemian, Quaternary Sci. Rev., 103, 91–115, 2014.

Chang, W., Applegate, P. J., Haran, M., and Keller, K.: Probabilistic calibration of a Greenland Ice Sheet model using spatially resolved synthetic observations: toward projections of ice mass loss with uncertainties, Geosci. Model Dev., 7, 1933–1943, doi:10.5194/gmd-7-1933-2014, 2014.

Chang, W., Haran, M., Applegate, P., and Pollard, D.: Calibrating an ice sheet model using high-dimensional non-Gaussian spatial data, J. Amer. Stat. Assoc., in press, http://arxiv.org/abs/1501.01937, v5, last access: 3 September 2015a.

Chang, W., Haran, M., Applegate, P., and Pollard, D.: Improving ice sheet model calibration using paleo and modern observations: a reduced dimensional approach, Annals Appl. Stat., in review, available at: http://arxiv.org/abs/1510.01676, v1, 6 October 2015b.

Chaput, J., Aster, R., Huerta, A., Sun, X., Lloyd, A., Wiens, D., Nyblade, A., Anandakishnan, S., Winberry, P., and Wilson, T.: The crustal thickness of West Antarctica, J. Geophys. Res., 119, 1–18, doi:10.1002/2013JB010642, 2014.

Clark, P. U. and Tarasov, L.: Closing the sea level budget at the Last Glacial Maximum, P. Natl. Acad. Sci. USA, 111, 15861–15862, 2014.

GMDD
8, 9925–9963, 2015

Cornford, S. L., Martin D. F., Graves, D. T., Ranken, D. F., Le Brocq, A. M., Gladstone, R. M., Payne, A. J., Ng, E. G., and Lipscomb, W. H.: Adaptive mesh, finite volume modeling of marine ice sheets, J. Comp. Phys., 232, 529–549, 2013.

DeConto, R. M. and Pollard, D.: Antarctica's contribution to Last Interglacial and future sea-level rise, Nature, in review, 2015.

DeConto, R. M., Pollard, D., and Kowalewski, D.: Modeling Antarctic ice sheet and climate variations during Marine Isotope Stage 31, Glob. Plan. Change, 88–89, 45–52, 2012.

Deschamps, P., Durand, N., Bard, E., Hamelin, B., Camoin, G., Thomas, A. L., Henderson, G. M., Okuno, J., and Yokoyama, Y.: Ice-sheet collapse and sea-level rise at the Bolling warming 14,600 years ago, Nature, 483, 559–564, 2012.

Docquier, D., Pollard, D., and Pattyn, F.: Thwaites Glacier grounding-line retreat: influence of width and buttressing parameterizations, J. Glaciol., 60, 305–313, 2014.

Durand, G., Gagliardini, O., Favier, L., Zwinger, T., and le Meur, E.: Impact of bedrock description on modeling ice sheet dynamics, Geophys. Res. Lett., 38, L20501, doi:10.1029/2011GL048892, 2011.

Dutrieux, P., De Rydt, J., Jenkins, A., Holland, P. R., Ha, H. K., Lee, S. H., Steig, E. J., Ding, Q., Abrahamsen, E. P., and Schröder, M.: Strong sensitivity of Pine Island ice-shelf melting to climatic variability, Science, 373, 174–178, 2014.

Favier, L., Gagliardini, O., Durand, G., and Zwinger, T.: A three-dimensional full Stokes model of the grounding line dynamics: effect of a pinning point beneath the ice shelf, The Cryosphere, 6, 101–112, doi:10.5194/tc-6-101-2012, 2012.

Favier, L., Durand, G., Cornford, S. L., Gudmundsonn, G. H., Gagliardini, O., Gillet-Chaulet, F., Zwinger, T., Payne, A. J., and Le Brocq, A. M.: Retreat of Pine Island Glacier controlled by marine ice-sheet instability, Nature Clim. Change, 4, 117–121, 2014.

Fretwell, P., Pritchard, H. D., Vaughan, D. G., Bamber, J. L., Barrand, N. E., Bell, R., Bianchi, C., Bingham, R. G., Blankenship, D. D., Casassa, G., Catania, G., Callens, D., Conway, H., Cook, A. J., Corr, H. F. J., Damaske, D., Damm, V., Ferraccioli, F., Forsberg, R., Fujita, S., Gim, Y., Gogineni, P., Griggs, J. A., Hindmarsh, R. C. A., Holmlund, P., Holt, J. W., Jacobel, R. W., Jenkins, A., Jokat, W., Jordan, T., King, E. C., Kohler, J., Krabill, W., Riger-Kusk, M., Langley, K. A., Leitchenkov, G., Leuschen, C., Luyendyk, B. P., Matsuoka, K., Mouginot, J., Nitsche, F. O., Nogi, Y., Nost, O. A., Popov, S. V., Rignot, E., Rippin, D. M., Rivera, A., Roberts, J., Ross, N., Siegert, M. J., Smith, A. M., Steinhage, D., Studinger, M., Sun, B., Tinto, B. K., Welch, B. C., Wilson, D., Young, D. A., Xiangbin, C., and Zirizzotti, A.:

GMDD
8, 9925–9963, 2015

Bedmap2: improved ice bed, surface and thickness datasets for Antarctica, The Cryosphere, 7, 375–393, doi:10.5194/tc-7-375-2013, 2013.
Gladstone, R. P., Lee, V., Rougier, J., Payne, A. J., Hellmer, H., LeBrocq, A. M., Shepherd, A., Edwards, T. L., Gregory, J., and Cornford, S.: Calibrated prediction of Pine Island Glacier retreat during the 21st and 22nd centuries with a coupled flowline model, Earth Planet. Sc. Lett., 333–334, 191–199, 2012.
Gohl, K., Uenzelmann-Neben, G., Larter, R. D., Hillenbrand, C.-D., Hochmuth, K., Kalberg, T., Weigelt, E., Davy, B., Kuhn, G., and Nitsche, F. O.: Seismic stratigraphic record of the Amundsen Sea Embayment shelf from pre-glacial to recent times: evidence for a dynamic West Antarctic ice sheet, Marine Geol., 344, 115–131, 2013.
Golledge, N. R., Fogwill, C. J., Mackintosh, A. N., and Buckley, K. M.: Dynamics of the last glacial maximum Antarctic ice-sheet and its response to ocean forcing, P. Natl. Acad. Sci. USA, 109, 16052–16056, 2012.
Golledge, N. R., Levy, R. H., McKay, R. M., Fogwill, C. J., White, D. A., Graham, A. G. C., Smith, J. A., Hillenbrand, C.-D., Licht, K. J., Denton, G. H., Ackert Jr., R. P., Maas, S. M., and Hall, B. L.: Glaciology and geological signature of the Last Glacial Maximum Antarctic ice sheet, Quaternary Sci. Rev., 78, 225–247, 2013.
Golledge, N. R., Menviel, L., Carter, L., Fogwill, C. J., England, M. H., Cortese, G., and Levy, R. H.: Antarctic contribution to meltwater pulse 1A from reduced Southern Ocean overturning, Nature Comm., 5, 5107, doi:10.1038/ncomms6107, 2014.
Gomez, N., Pollard, D., and Mitrovica, J. X.: A 3-D coupled ice sheet-sea level model applied to Antarctica through the last 40 ky, Earth Plan. Sci. Lett., 384, 88–99, 2013.
Gomez, N., Pollard, D., and Holland, D.: Sea level feedback lowers projections of future Antarctic Ice Sheet mass loss, Nature Commun., 6, 8798, doi:10.1038/ncomms9798, 2015.
He, F., Shakun, J. D., Clark, P. U., Carlson, A. E., Liu, Z., Otto-Bliesner, B. L., and Kutzbach, J. E.: Northern Hemisphere forcing of Southern Hemisphere climate during the last deglaciation, Nature, 494, 81–85, 2013.
Hellmer, H., Kauker, F., Timmermann, R., Determann, J., and Rae, J.: Twenty-first-century warming of a large Antarctic ice-shelf cavity by a redirected coastal current, Nature, 485, 225–228, 2012.
Holland, P. R., Jenkins, A., and Holland, D. M.: The response of ice shelf basal melting to variations in ocean temperature, J. Climate, 21, 2558–2572, 2008.

GMDD
8, 9925–9963, 2015

Holschuh, N., Pollard, D., Anandakrishnan, S., and Alley, R.: Evaluating Marie Byrd Land stability using an improved basal topography, Earth Plan. Sci. Lett., 408, 362–369, 2014.
Huybrechts, P.: Sea-level changes at the LGM from ice-dynamic reconstructions of the Greenland and Antarctic ice sheets during the glacial cycles, Quaternary Sci. Rev., 21, 203–231, 2002.
Jakobsson, M., Anderson, J. B., Nitsche, F. O., Dowdeswell, J. A., Gyllencreutz, R., Kirchner, N., Mohammad, R., O'Regan, M., Alley, R. B., Anandakrishnan, S., Eriksson, B., Kirshner, A., Fernandez, R., Stolldorf, T., Minzoni, R., and Majewski, W.: Geological record of ice shelf break-up and grounding line retreat, Pine Island Bay, West Antarctica, Geology, 39, 691–694, 2011.
Joughin, I., Smith, B. E., and Medley, B.: Marine ice sheet collapse potentially under way for the Thwaites Glacier basin, West Antarctica, Science, 344, 735–738, 2014.
Konrad, H., Sasgen, S., Pollard, D., and Klemann, V.: Potential of the solid-Earth response for limiting long-term West Antarctic Ice Sheet retreat in a warming climate, Earth Plan. Sci. Lett., 432, 254–264, 2015.
Le Brocq, A. M., Payne, A. J., and Vieli, A.: An improved Antarctic dataset for high resolution numerical ice sheet models (ALBMAP v1), Earth Syst. Sci. Data, 2, 247–260, doi:10.5194/essd-2-247-2010, 2010.
Liu, Z., Otto-Bliesner, B. L., He, F., Brady, E. C., Tomas, R., Clark, P. U., Carlson, A. E., Lynch-Stieglitz, J., Curry, W., Brook, E., Erickson, D., Jacob, R., Kutzbach, J., and Cheng, J.: Transient simulation of last deglaciation with a new mechanism for Bølling-Allerød warming, Science, 325, 310–314, 2009.
Mackintosh, A., Golledge, N., Domack, E., Dunbar, R., Leventer, A., White, D., Pollard, D., DeConto, R., Fink, D., Zwartz, D., Gore, D., and Lavoie, C.: Retreat of the East Antarctic ice sheet during the last glacial termination, Nature Geosci., 4, 195–202, 2011.
Maris, M. N. A., van Wessem, J. M., van de Berg, W. J., de Boer, B., and Oerlemans, J.: A model study of the effect of climate and sea-level change on the evolution of the Antarctic Ice Sheet from the Last Glacial Maximum to 2100, Clim. Dynam., 45, 837–851, 2015.
McNeall, D. J., Challenor, P. G., Gattiker, J. R., and Stone, E. J.: The potential of an observational data set for calibration of a computationally expensive computer model, Geosci. Model Dev., 6, 1715–1728, doi:10.5194/gmd-6-1715-2013, 2013.
Meinshausen, M., Smith, S. J., Calvin, K., Daniel, J. S., Kainuma, M. L. T., Lamarque, J.-F., Matsumoto, K., Montzka, S. A., Raper, S. C. B., Riahi, K., Thomson, A., Velders, G. J. M.,

GMDD
8, 9925–9963, 2015

and van Vuuren, D. P. P.: The RCP greenhouse gas concentrations and their extensions from 1765 to 2300,. Clim. Change, 109, 213–241, 2011.

Mercer, J. H.: West Antarctic ice sheet and CO_2 greenhouse effect: a threat of disaster, Nature, 271, 321–325, 1978.

Morlighem, M., Rignot, E., Seroussi, H., Larour, E., Ben Dhia, H., and Aubry, D: Spatial patterns of basal drag inferred using control methods from a full-Stokes and simpler models for Pine Island Glacier, West Antarctica, Geophys. Res. Lett., 37, L14502, doi:10.1029/2010GL043853, 2010.

Morlighem, M., Seroussi, H., Larour, E., and Rignot, E.: Inversion of basal friction in Antarctica using exact and incomplete adjoints of a higher-order model, J. Geophys. Res.-Earth Surface, 3, 1746–1753, 2013.

Nick, F. M., van der Veen, C. J., Vieli, A., and Benn, D. I.: A physically based calving model applied to marine outlet glaciers and implications for the glacier dynamics, J. Glaciol., 56, 781–794, 2010.

Parizek, B. R., Christianson, K., Anandakrishnan, S., Alley, R. B., Walker, R. T., Edwards, R. A., Wolfe, D. S., Bertini, G. T., Rinehart, S. K., Bindschadler, R. A., and Nowicki, S. M. J.: Dynamic (in)stability of Thwaites Glacier, West Antarctica, J. Geophys. Res.-Earth Surface, 118, 638–655, 2013.

Pattyn, F., Perichon, L., Durand, G., Favier, L., Gagliardini, O., Hindmarsh, R. C. A., Zwinger, T., Albrecht, T., Cornford, S., Docquier, D., Furst, J. J., Goldberg, D., Gudmundsson, G. H., Humbert, A., Hutten, M., Huybrechts, P., Jouvet, G., Kleiner, T., Larour, E., Martin, D., Morlighem, M., Payne, A. J., Pollard, D., Ruckamp, M., Rybak, O., Seroussi, H., Thoma, M., and Wilkens, N.: Grounding-line migration in plan-view marine ice-sheet models: results of the ice2sea MISMIP3d intercomparison, J. Glaciol., 59, 410–422, 2013.

Peltier, W. R.: Global glacial isostacy and the surface of the ice-age Earth: the ICE-5G (VM2) model and GRACE, Ann. Rev. Earth Planet. Sci., 32, 111–149, 2004.

Philippon, G., Ramstein, G., Charbit, S. Kageyama, M., Ritz, C., and Dumas. C.: Evolution of the Antarctic ice sheet throughout the last deglaciation: a study with a new coupled climate – north and south hemisphere ice sheet model, Earth Plan. Sci. Lett., 248, 750–758, 2006.

Pollard, D. and DeConto, R. M.: Modelling West Antarctic ice sheet growth and collapse through the past five million years, Nature, 458, 329–332, 2009.

Pollard, D. and DeConto, R. M.: Description of a hybrid ice sheet-shelf model, and application to Antarctica, Geosci. Model Dev., 5, 1273–1295, doi:10.5194/gmd-5-1273-2012, 2012a.

GMDD

8, 9925–9963, 2015

Pollard, D. and DeConto, R. M.: A simple inverse method for the distribution of basal sliding coefficients under ice sheets, applied to Antarctica, The Cryosphere, 6, 953–971, doi:10.5194/tc-6-953-2012, 2012b.

Pollard, D., DeConto, R. M., and Alley, R. B.: Potential Antarctic Ice Sheet retreat driven by hydrofracturing and ice cliff failure, Earth Plan. Sci. Lett., 412, 112–121, 2015a.

Pollard, D., DeConto, R., Chang, W., Haran, M., and Applegate, P.: Large ensemble modeling of the Antarctic Ice Sheet: contributions to past and future sea-level rise, The Cryosphere Discuss., in preparation, 2015b.

Pritchard, H. D., Ligtenberg, S. R. M., Fricker, H. A., Vaughan, D. G., van den Broeke, M. R., and Padman, L.: Antarctic ice-sheet loss driven by basal melting of ice shelves, Nature, 484, 502–505, 2012.

Ritz, C., Rommelaere, V., and Dumas, C.: Modeling the evolution of Antarctic ice sheet over the last 420,000 years: implications for altitude changes in the Vostok region, J. Geophys. Res.-Atmos., 106, 31943–31964, 2001.

Rignot, E., Mouginot, J., Morlighem, M., Seroussi, H., and Scheuchl, B: Widespread, rapid grounding line retreat of Pine Island,Thwaites, Smith, and Kohler glaciers, West Antarctica, from 1992 to 2011, Geophys. Res. Lett., doi:10.1002/2014GL060140, 3502–3509, 2014.

Schoof, C.: Ice sheet grounding line dynamics: steady states, stability, and hysteresis, J. Geophys. Res.-Earth Surf., 112, F03S28, doi:10.1029/2006JF000664, 2007.

Shepherd, A., Ivins, E. R., A. G., Barletta, V. R., Bentley, M. J., Bettadpur, S., Briggs, K. H., Bromwich, D. H., Forsberg, R., Galin, N., Horwath, M., Jacobs, S., Joughin, I., King, M. A., Lenaerts, J. T. M., Li, J., Ligtenberg, S. R. M., Luckman, A., Luthcke, S. B., McMillan, M., Meister, R., Milne, G., Mouginot, J., Muir, A., Nicolas, J. P., Paden, J., Payne, A. J., Pritchard, H., Rignot, E., Rott, H., Sorensen, L. S., Scambos, T. A., Scheuchl, B., Schrama, E. J. O., Smith, B., Sundal, A. V., van Angelen, J. H., van de Berg, W. J., van den Broeke, M. R., Vaughan, D. G., Velicogna, I., Wahr, J., Whitehouse, P. L., Wingham, D. J., Yi, D., Young, D., and Zwally, H. J.: A reconciled estimate of ice-sheet mass balance, Science, 338, 1193–1198, 2012.

Smith, J. A., Hillenbrand, C.-D., Kuhn, G., Klages, J. P., Graham, A. G. C., Larter, R. T., Ehrmann, W., Moreton, S. G., Wiers, S., and Frederichs, T.: New constraints on the timing of West Antarctic Ice Sheet retreat in the eastern Amundsen Sea since the last Glacial Maximum, Glob. Planet. Change, 122, 224–237, 2014.

GMDD
8, 9925–9963, 2015

Stone, E. J., Lunt, D. J., Annan, J. D., and Hargreaves, J. C.: Quantification of the Greenland ice sheet contribution to Last Interglacial sea level rise, Clim. Past, 9, 621–639, doi:10.5194/cp-9-621-2013, 2013.

Tarasov, L., Dyke, A. S., Neal, R. M., and Peltier, W. R.: A data-calibrated distribution of deglacial chronologies for the North American ice complex from glaciological modeling, Earth Plan. Sci. Lett., 315–316, 30–40, 2012.

The RAISED Consortium: A community-based geological reconstruction of Antarctic Ice Sheet deglaciation since the Last Glacial Maximum, Quaternary Sci. Rev., 100, 1–9, 2014.

Urban, N. M. and Fricker, T. E.: A comparison of Latin hypercube and grid ensemble designs for the multivariate emulation of an Earth System model, Comput. Geosci., 36, 746–755, 2010.

Vaughan, D. G.: West Antarctic Ice Sheet collapse: the fall and rise of a paradigm, Clim. Change, 91, 65–79, 2008.

Weber, M. E., Clark, P. U., Kuhn, G., Timmermann, A., Sprenk, D., Gladstone, R., Zhang, X., Lohmann, G., Menviel, L., Chikamoto, M. O., Friedrich, T., and Ohlwein, C.: Millennial-scale variability in Antarctic ice-sheet discharge during the last deglaciation, Nature, 510, 134–138, 2014.

Weertman, J.: Stability of the junction of an ice sheet and an ice shelf, J. Glaciol., 13, 3–11, 1974.

Whitehouse, P. L., Bentley, M. J., and Le Brocq, A. M.: A deglacial model for Antarctica: geological constraints and glaciological modeling as a basis for a new model of Antarctic glacial isostatic adjustment, Quaternary Sci. Res., 32, 1–24, 2012a.

Whitehouse, P. L., Bentley, M. J., Milne, G. A., King, M. A., and Thomas, I. D.: A new glacial isostatic model for Antarctica: calibrated and tested using observations of relative sea-level change and present-day uplifts, Geophys. J. Int., 190, 1464–1482, 2012b.

GMDD
8, 9925–9963, 2015

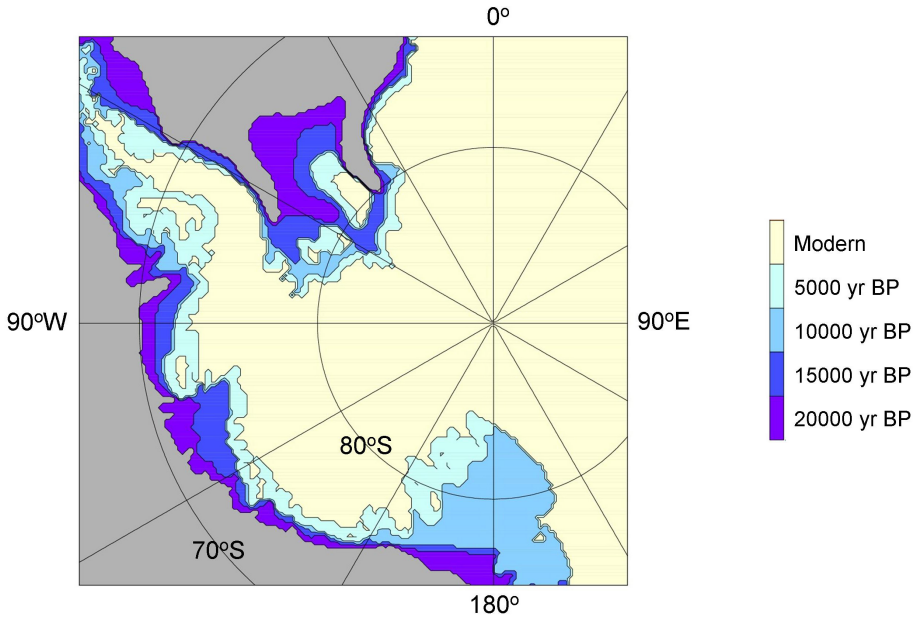

Figure 1. Geographical map of West Antarctica. Light yellow shows the modern extent of grounded ice (using Bedmap2 data; Fretwell et al., 2013). Blue and purple areas show expanded grounded-ice extents at 5, 10, 15 and 20 ka (thousands of years before present) reconstructed by the RAISED consortium (2014), plotted using their vertex information (S. Jamieson, personal communication, 2014), and choosing their Scenario A for the Weddell embayment. These maps are used in the large ensemble scoring (TOTE, TROUGH and GL2D data types, Sect. 2.3).

GMDD
8, 9925–9963, 2015

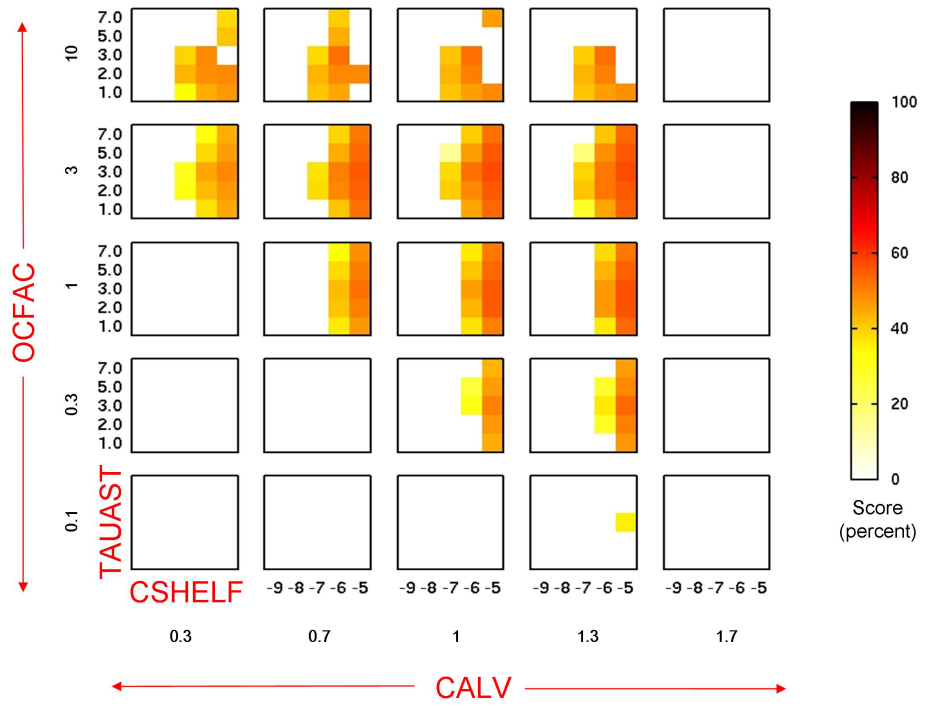

Figure 2. Aggregate scores for the complete large ensemble suite of runs (625 runs, 4 model parameters, 5 values each), used in the simple method with score-weighted averaging. The score values range from 0 (white, no skill) to 100 (dark red, perfect fit). The figure is organized to show the scores in the four-dimensional space of parameter variations. The four parameters are: CSHELF = basal sliding coefficient in modern oceanic areas (exponent x, $10^{-x}\,\mathrm{m\,a^{-1}\,Pa^{-2}}$). TAUAST = e-folding time of bedrock-elevation isostatic relaxation (kyrs). OCFAC = oceanic-melt-rate coefficient at base of floating ice shelves (non-dimensional). CALV = calving-rate factor at edge of floating ice shelves (non-dimensional). Since each parameter only takes 5 values, the results are blocky, but effectively show the behavior of the score over the full range of plausible parameter values.

GMDD
8, 9925–9963, 2015

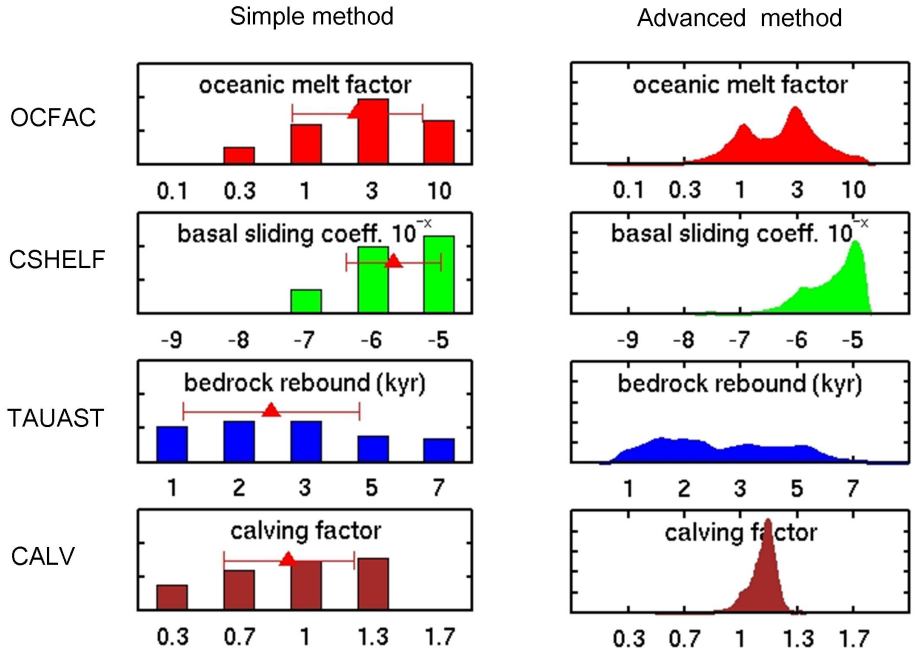

Figure 3. Left-hand panels: Ensemble-mean scores for individual parameter values, using the simple averaging method. The red triangle shows the mean, and whiskers show the 1 sigma standard deviations. Right-hand panels: Probability densities for individual parameters, using the advanced statistical techniques in Chang et al. (2015b) extended as described in Sect. 2.5 and Appendix C.

GMDD
8, 9925–9963, 2015

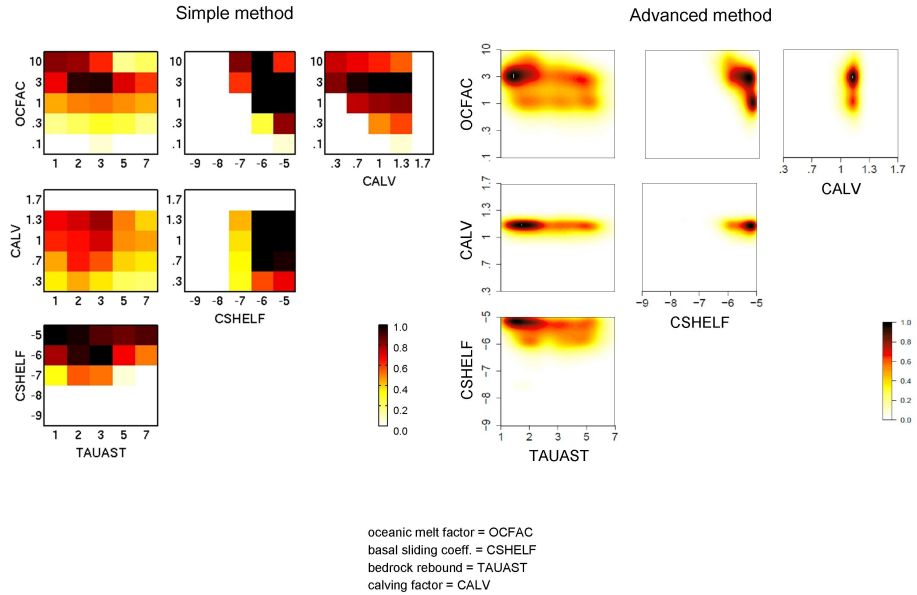

Figure 4. Left-hand panels: Ensemble-mean scores for pairs of parameters, using the simple averaging method. Right-hand panels: Probability densities for pairs of parameters, using the advanced statistical techniques in Chang et al. (2015b) extended as described in Sect. 2.5 and Appendix C.

GMDD
8, 9925–9963, 2015

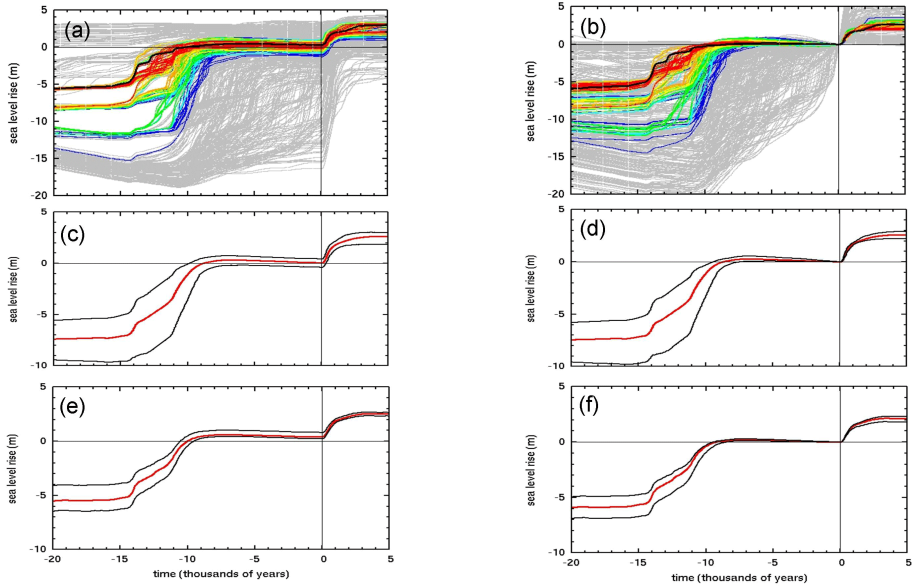

GMDD
8, 9925–9963, 2015

Large ensemble modeling of last deglacial retreat of the West Antarctic Ice Sheet

D. Pollard et al.

Figure 5. Equivalent global-mean sea level rise (ESL) vs. time. Time runs from 20 000 years before present to 5000 years after present. ESL changes are calculated from the total ice amount in the domain divided by global ocean area, allowing for less contribution from ice grounded below sea level. The runs are extended 5000 years into the future with idealized linearly ramped climate warming. **(a)** Scatter plot of all 625 individual runs in the LE. ESL amounts are calculated relative to modern observed Antarctica, so non-zero values at time = 0 imply departures from the observed ice state. Grey curves are for runs with aggregate score $S = 0$, and colored curves are for $S > 0$ in descending S order with 25 curves per color (red, orange, yellow, green, cyan, blue in descending order). The best scoring individual run is shown by a thick black curve (OCFAC = 3, CALV = 1, CSHELF = −5, TAUAST = 3, with $S = 0.570$). **(b)** As **(a)** but with ESL amounts relative to each run's modern value, so the curves pass exactly through zero at time = 0. **(c)** Score weighted curves over the whole LE, using the simple statistical method. Red curve is the score-weighted mean, i.e., $\Sigma\{S^{(n)}\mathrm{ESL}^{(n)}(t)\}/\Sigma\{S^{(n)}\}$ where $S^{(n)}$ is the aggregate score for run n, $\mathrm{ESL}^{(n)}(t)$ is the equivalent sea-level rise for run n at time t., and the sums are over all n (1 to 625) in the LE. Black curves show the one-sided standard deviations, i.e., the root mean square of deviations for $\mathrm{ESL}^{(n)}$ above the mean (upper curve) or below the mean (lower curve) at each time t. $\mathrm{ESL}^{(n)}(t)$ are relative to modern observed Antarctica, as in panel **(a)**. **(d)** As **(c)** but with $\mathrm{ESL}^{(n)}(t)$ relative to each run's modern value as in **(b)**. **(e)** and **(f)**: Corresponding results to **(c)** and **(d)** respectively, using the advanced statistical techniques in Chang et al. (2015b) extended as described in Sect. 2.5 and Appendix C.

GMDD
8, 9925–9963, 2015

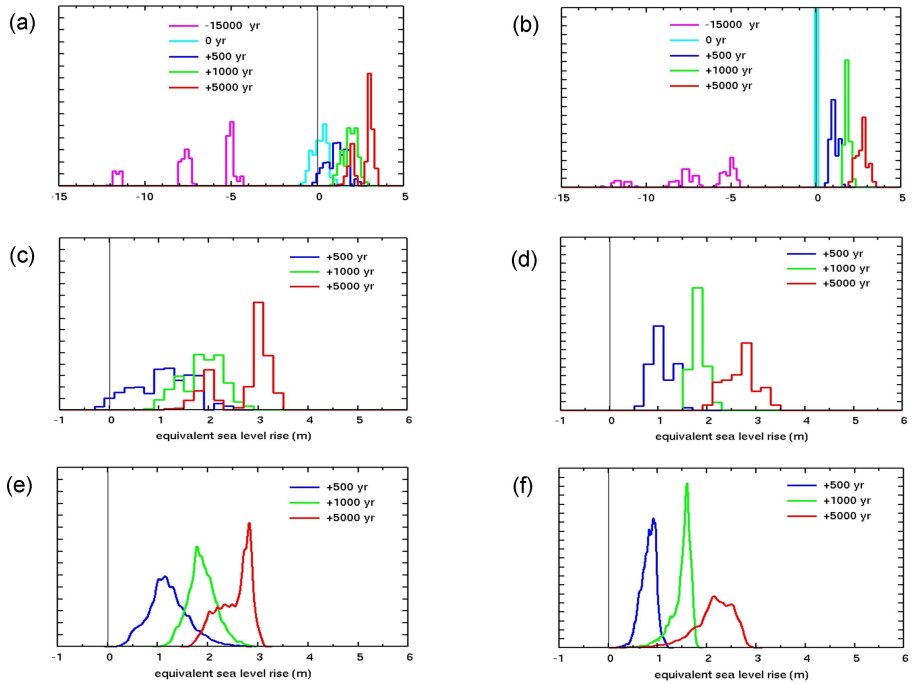

Figure 6. (a) Probability densities of equivalent sea level (ESL) rise at particular times in the LE simulations, computed with the simple averaging method. At a given time t, the density $P(E)$ is the sum of aggregate scores $S^{(n)}$ for all runs n with equivalent sea-level rise $\mathrm{ESL}^{(n)}(t)$ within the bin $E-0.1$ to $E+0.1$ m, i.e., using equispaced bins 0.2 m wide. The resulting $P(E)$ are normalized so that the integral with respect to E is 1. $\mathrm{ESL}^{(n)}(t)$ are relative to modern observed Antarctica, as in Fig. 5a. **(b)** As **(a)** but with $\mathrm{ESL}^{(n)}(t)$ relative to each run's modern value, as in Fig. 5b. **(c)** and **(d)**: As **(a)** and **(b)** respectively, but only showing times +500, +1000 and +5000 years after present. **(e)** and **(f)**: Corresponding results to **(c)** and **(d)** respectively, using the advanced statistical techniques in Chang et al. (2015b) extended as described in Sect. 2.5 and Appendix C.

GMDD
8, 9925–9963, 2015

The 4 parameters varied in the large ensemble, and their 5 values.

OCFAC: Sub-ice oceanic melt coefficient.
Values are 0.1, 0.3, 1, 3, 10 (non-dimensional).
Corresponds to K in Eq. 17 of Pollard and Deconto (2012a).

CALV: Factor in calving of icebergs at oceanic edge of floating ice shelves.
Values are 0.3, 0.7, 1, 1.3, 1.7 (non-dimensional).
Multiplies combined crevasse-depth-to-ice-thickness ratio r in Eq. B7 of Pollard et al. (2015a).

CSHELF: Basal sliding coefficient for ice grounded on modern-ocean beds.
Values are 10^{-9}, 10^{-8}, 10^{-7}, 10^{-6}, 10^{-5} (m yr^{-1} Pa^{-2}).
Corresponds to C in Eq. 11 of Pollard and Deconto (2012a).

TAUAST: e-folding time of bedrock relaxation towards isostatic equilibrium.
Values are 1, 2, 3, 5, 7 kyrs.
Corresponds to τ in Eq. 33 of Pollard and Deconto (2012a).

Listing 1.

GMDD
8, 9925–9963, 2015

Data types used in evaluating model simulations.

1. TOTE: Modern grounding-line locations.
Misfit M_1: based on total area of model-data mismatch for grounded ice.
Data: Bedmap2 (Fretwell et al., 2013).

2. TOTI: Modern floating ice-shelf locations.
Misfit M_2: based on total area of model-data mismatch for floating ice.
Data: Bedmap2 (Fretwell et al., 2013).

3. TOTDH: Modern grounded ice thicknesses.
Misfit M_3: based on RMS model-data difference of grounded ice thicknesses.
Data: Bedmap2 (Fretwell et al., 2013).

4. TROUGH: Past grounding-line distance vs. time along the centerline trough of Pine Island Glacier. Centerline data for the Ross and Weddell basins can also be used, but not in this study.
Misfit M_4: based on RMS model-data difference over the period 20 to 0 ka.
Data: RAISED (2014).

5. GL2D: Past grounding-line locations (see Fig. 1). Only the Amundsen Sea region is used in this study.
Misfit M_5: based on model-data mismatches for 20, 15, 10, 5 ka.
Data: RAISED (2014).

6. RSL: Past Relative Sea Level (RSL) records.
Misfit M_6 : based on χ-squared measure of model-data differences at individual sites.
Data: compilation in Briggs and Tarasov (2013).

7. ELEV/DSURF: Past cosmogenic elevation vs. age (ELEV) and thickness vs. age (DSURF).
Misfits M_{7a}, M_{7b}: based on model-data differences at individual sites, combined as in Appendix B.
Data: compilations in Briggs and Tarasov (2013) for ELEV, in RAISED (2014) for DSURF.

8. UPL: Modern uplift rates on rock outcrops.
Misfit M_8: based on RMS model-data difference at individual sites.
Data: compilation in Whitehouse et al. (2012b).

Listing 2.

GMDD
8, 9925–9963, 2015